

STUDY ON BALL END MILLING PROCESS USING TWO DIMENSIONAL FINITE ELEMENT METHOD

Ahmad Shahir Jamaludin*, Abdullah Yassin and Mohd. Shahril Osman

Department of Mechanical and Manufacturing Engineering,
Faculty of Engineering,
Universiti Malaysia Sarawak,
94300 Kota Samarahan, Sarawak

ABSTRACT

In this paper, finite element analysis on laser sintered material machining with predicted cutting force and temperature distribution is explained. The process involved 2D orthogonal down-cut milling with the application of two dimension thermo mechanical plane strain model. The updated Lagrangian formulation was used whereas cutting simulation does not involved element separation but automatic remesh when element distorted critically. AISI 1055 mild steel properties were used as comparison. Various types of friction models were adopted in obtaining precise results. Predicted cutting force and cutting edge temperature are validated against corresponding experimental values by previous researches. From the simulation results, the shear friction model of 0.8 is the optimum friction model whereas 5-15% errors were obtained for increasing machining radial depth for AISI 1055. Lower cutting force predicted for laser sintered materials as compared to AISI 1055 due to lower Young modulus value. Cutting edge temperature predicted for laser sintered materials is higher due to its low thermal conductivity as compared to AISI 1055.

Keywords: *Finite element method (FEM), 2D orthogonal end milling, cutting force prediction, cutting temperature prediction, friction model*

1.0 INTRODUCTION

Injection moulding is one of the most versatile and important operations for mass production of complex plastic parts with excellent dimensional tolerance. In the conventional mould manufacturing, subtractive processes such as high speed machining (HSM) [1] and electro discharge machining (EDM) are applied to make the mould from hardened steel [2]. This conventional mould manufacturing is not economic due to these subtractive processes are time consuming. Production time is one of the key successfully factors in the consumer product marketplace. Various negative effects such as chatter, wobble and impact loading cause by the deflection at the cutting edge in making a precise mould in which having a deep rib could result poor dimensional accuracy. The easiest way to control the tool deflection is by reducing the tool length. Therefore, this conventional mould manufacturing is not suitable in making a complicated injection mould.

Stereolithography (SL) application has reduced mould manufacturing production time and cost [3]. Furthermore, a mould having a deep rib can be created. However, due to its low flexural stresses, life span of the mould produce from SL is short [3]. By Introducing Selective Laser Sintering (SLS) with application of laser beam to irradiate

*Corresponding author : aero_zephyr@yahoo.com

metal powder in making three dimensional shaped parts could greatly reduce mould manufacturing time and increase its life span. However, resulting part offers limited dimensional accuracy and poor surface roughness [4].

Milling-combined laser sintering system (MLSS) that combines laser sintering of fine metallic powder and high speed milling has been developed to overcome these deficiencies. Small ball end mill is employed to machine complicated mould features because ball end mill capable in machining free-form surfaces [5]. Therefore, making complicated mould having a deep rib is feasible and the dimensional accuracy is also can be improved.

In MLSS, about 30% from the total production time in making a mould is required for high speed machining (HSM) [6, 7]. According to Abe *et al.*, machinability study of laser-sintered material did not attract much attention from the researchers [6, 7]. Therefore, any potential-advantage of MLSS as a new invention in mould making, there will be required further study on machinability of laser sintered materials. In this study, machinability of laser sintered material will be analyzed by mean estimated cutting force and cutting temperature of the machining process.

MLSS process consist of two alternating processes, which are forming a layer profile by laser sintering and surface finishing by high speed milling. CAD designed 3-D model is divided into 50 μm thickness sliced layers transferred to the MLSS. A sandblasted steel base plate is placed on the building platform prior to the laser sintering process. A recoating blade is used to spread loose metallic powder into layer with predetermined thickness of 50 μm . The surface of loose metallic powder layer is then being irradiated by the laser beam to produce a layer-wise profile according to the CAD data. After forming a few layers, the rough and finish milling process is executed at the periphery surface. These sintering and milling processes at the periphery surface are repeated whereas top surface is not cut after all layers are sintered.

1.1 Finite Element Method (FEM)

Finite element method (FEM) is a numerical technique which can be used to model and simulate real world problems. Finite element method (FEM) has become famous in simulating high speed machining and useful in saving cost, time, and capable to forecast effects of cutting parameter on cutting force, cutting edge temperature and chip formations[10,11]. Through the application of FEM, cutting forces and temperatures obtained can be used in estimating the optimum cutting conditions such as cutting speed, cutting depth, etc.

One of the most simplified models of FEM for machining is orthogonal cutting. Orthogonal cutting involved cutting edge moves perpendicular to the relative motion between cutting tool and workpiece to remove unwanted material from the workpiece with constant uncut chip thickness [10]. This model only suitable in simulating the turning processes whereas continuous chip with constant thickness that depends on the constant cutting feed. In milling processes, uncut chip thickness vary depends on fix parameters of radial depth, cutting tool diameter and cutting feed and cutting edge radial position [11].

Earlier researcher developed 2D orthogonal cutting such as Usui and Shirakashi obtained steady state cutting using iterative convergence method in FEM [12]. Strenkowski and Carroll developed numerical model without a preformed chip using updated Lagrangian code [13]. Recent 2D model developed by Özel [11] and Filice *et al.* [10] applied friction condition in obtaining more realistic data. Davim *et al.* studied plastic strain and plastic strain rate in machining AISI 1045 FEM simulation [14]. This investigation will applied updated Lagrangian formulation on two dimensional thermo mechanical plane strain FEM model.

Widely known materials such as mild steel AISI 1045 [10, 11, 14], aluminium (Al7075) [15], titanium alloy (Ti6Al-4V) [16] and AISI P20 mould steel alloy [17] was

performed in FEM machining simulation and have a significant agreement with experimental results. In this study, laser sintered material will be applied as main material properties and AISI 1055 will be the comparison. Yassin *et al.* studied the machinability of laser-sintered materials experimentally without FEM analysis [19]. Therefore, application of FEM could extend further the knowledge of MLSS and laser sintered material. Results obtained from FEM simulation will be compare with the experimental results for validation.

2.0 FINITE ELEMENT MODEL

Figure 1 shows apparatus for the experimental approach that previously performed by using two flute ball end mill by Yassin *et al.* [19]. This apparatus were then being modeled to 2D finite element model as shown in Figure 2. $10\mu\text{m}$ tool edge radius, r were used according to original cutting tool. This could define more realistic simulation to represent an actual experimental approach. This 2D finite element model was design in plane strain assumption due to the undeformed chip thickness is assumed small compare to the width of the cutting edge [17].

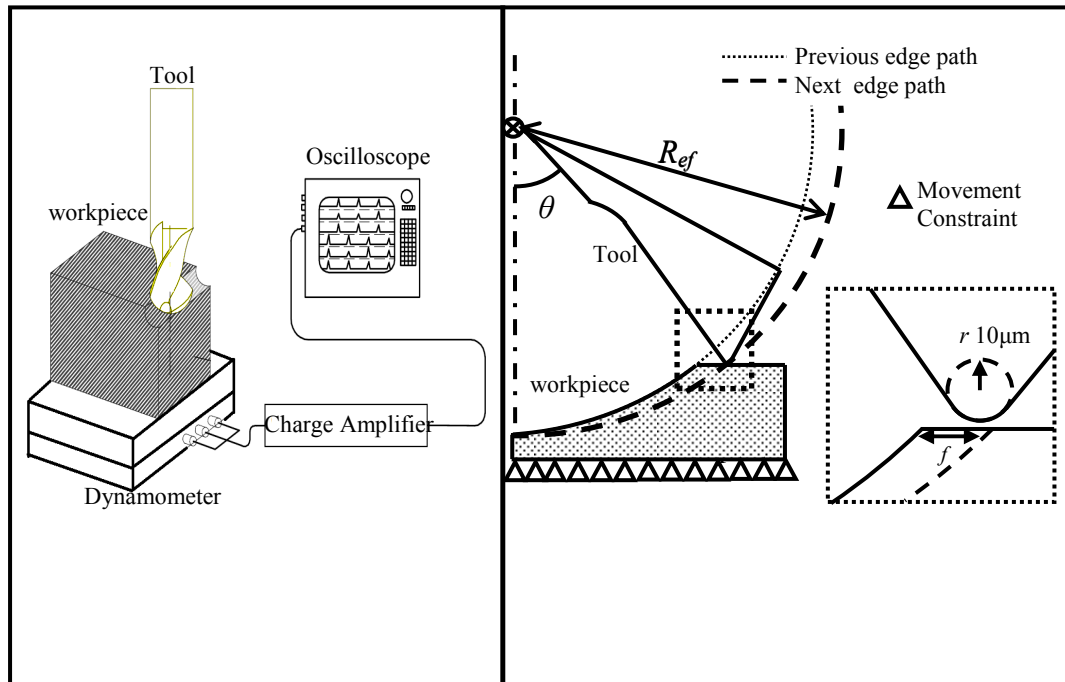


Figure 1 : Experimental procedure by Yassin *et al.* [19]

Figure 2 : Simplified tool and workpiece FEM model

Complicated ball part of the end mill was simplified whereas maximum effective radius was considered as cutting tool rotation radius in obtaining maximum cutting force and maximum cutting temperature. Peripheral milling is the process whereas teeth located on the periphery of the cutter body generates the milled surface. Figure 3 shows the diagram of peripheral milling process.

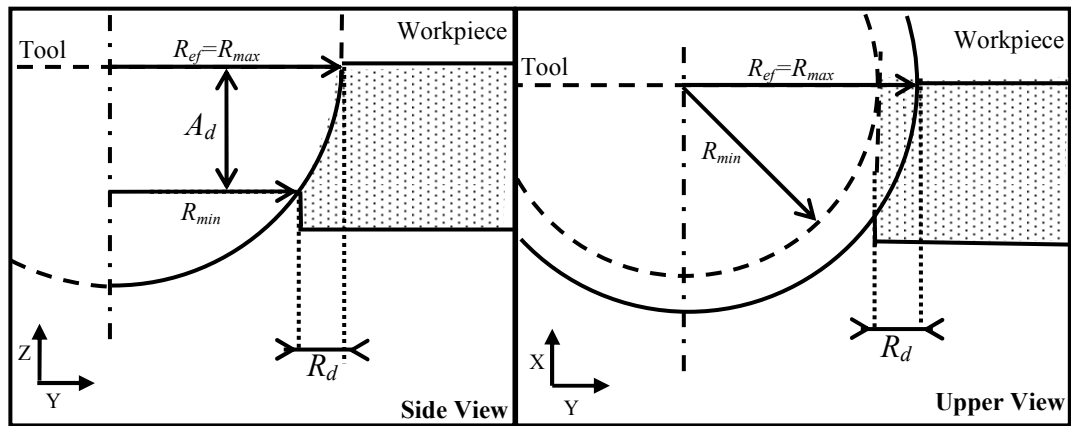


Figure 3: Peripheral milling with (left) side view and (right) upper view

2.1 Meshing

Figure 4 shows the overall tool and workpiece mesh for the study. Isoparametric quadrilaterals mesh and adapted remeshing technique were used to mesh the 2D FE model using commercially available FEA software. Isoparametric quadrilaterals mesh provide less element and capable to rotate arbitrarily [20]. Adapted remeshing technique capable to remesh the model if critical element distortion existed during the simulation and this technique does not required element separation [10, 11].

Denser and fine mesh was only applied at the tool edge – workpiece contact area representing as a main mechanical work and large elastic-plastic deformation was then generated. This meshing technique will ensure lighter and precise simulations can be performed for the study. 2000 elements were used for workpiece and 1000 elements were used for cutting tool mesh.

The cutting processes were assumed as an ideal with no cutters run-out (rigid). Workpiece will experience elastic-plastic deformation when cutting tool-workpiece contact was existed [10, 11].

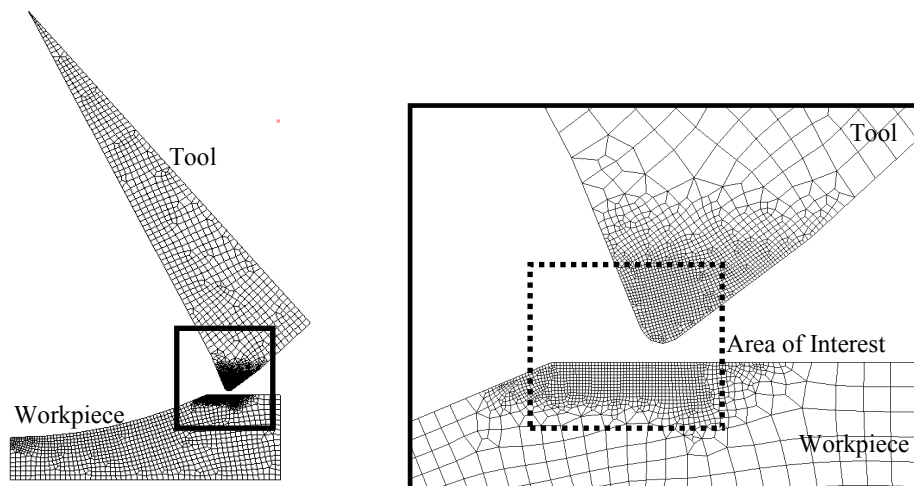


Figure 4 : Tool and workpiece mesh

2.2 Contact Length Assumptions

Kato *et al.* [21] contact length model were used as tool-workpiece contact length in the simulation as shown in equation 1. L_c is tool-workpiece contact length and h in the undeformed chip thickness

$$L_c = 2h \quad (1)$$

2.3 Friction Models

Frictional stress on rake face of tool is assumed constant and low stress variation of frictional stress, τ and normal stress, σ_n are neglected [11]. This can be expressed with following equation 2.

$$\tau = mk \quad (2)$$

m is friction factor from 0.6 to 0.9 and k is shear flow stress of the work material.

2.4 Heat Generation

Main heat sources are shown in Figure 5 [22]. In primary deformation zone (Zone 1), heat is generated due to plastic activity was performed at the shear plane. In the secondary shear zone (Zone 2), heat is generated due to work ended in chip deformation and sliding friction at the tool-chip interface. In the tertiary deformation zone (Zone 3), heat is generated due to rubbing friction contact between tool flank face and the newly machined surface.

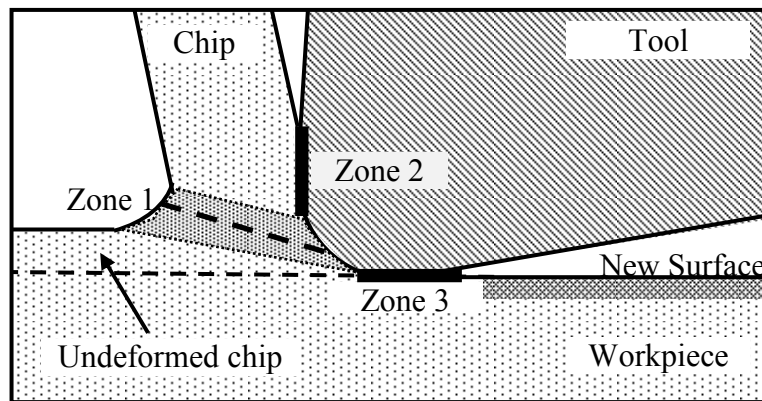


Figure 5: Main heat source during machining

In this study, all the mechanical work performs in the machining process is assumed fully converted into heat [22]. Heat generation Q_r (W) in the primary deformation zone is equal to the rate of energy consumption during metal cutting and shown by equation 3.

$$Q_r = W_c = F_v V \quad (3)$$

F_v (N) is the cutting force and V (m/sec) is the cutting speed. Heat generation due to metal cutting were separated between tool and workpiece then heat flux, q (W/mm²) may be calculated from the heat generation and contact area was obtained from the simulation as equation 4 [23].

$$q = Q_r / tb \quad (4)$$

t (mm) and b (mm) are contact length and cutting width.

2.5 Thermal Boundaries

Thermal boundary conditions are important in determining temperature gradient in metal cutting condition. In Figure 6, C'-C'' defined the tool-chip contact interface whereas the contact between tool and workpiece is assumed thermally ideal and a large value of $h=1000$ (kW/m²K) is employed according to Abukhshim *et al.* [24].

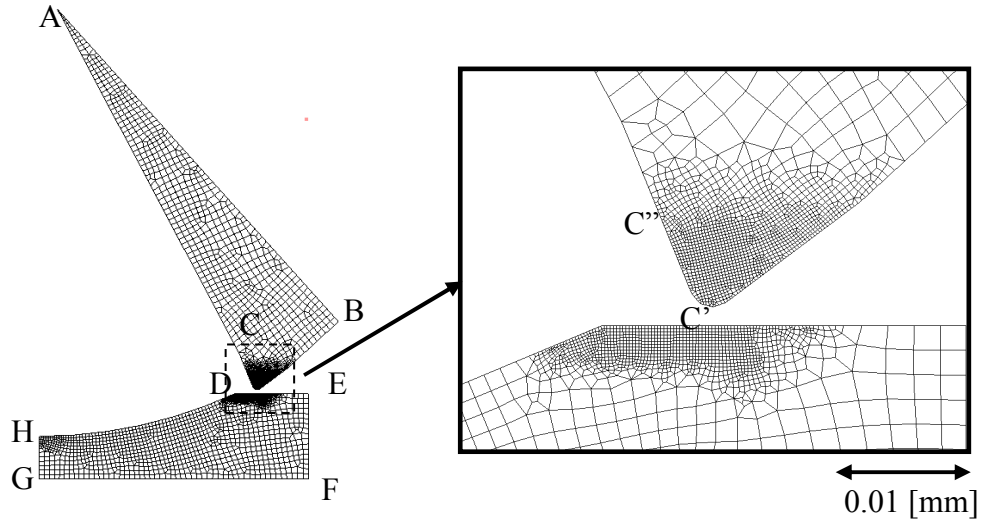


Figure 6 : Thermal boundaries on tool and workpiece

Heat loss of the tool and workpiece at free surface to the environment is defined to be caused by convection whereas heat convection coefficient of 20 (W/m²K) is employed to C''-A, D-E, H-D and B-C' according to Filice *et al.* [10].

The boundaries that are sufficiently far apart from the cutting zone is assumed to be not affected by temperature and thus, boundaries A-B, E-F and F-G are fixed with environment temperature, 20 (°C) according to Abukhshim *et al.* [24]. Heat loss due to radiation is neglected.

2.6 Data Collections

Figure 7 shows the schematic diagram of cutting tool and optical fiber position whereas cutting temperature values were measured by Yassin *et al.* [19]. In comparing the predicted cutting edge temperature with the experimental results, air cutting time and cooling effect have to be taken into consideration. According to Hosokawa *et al.* [25], the temperature at a given time after the tool finishes cutting the workpiece and revolves is given by

$$T_{\psi}(\delta) = (T_r - T_0)e^{-a\delta} + T_r \quad (5)$$

T_{ψ} (°C) is the temperature at a given air cutting time, T_r (°C) is the instantaneous cutting temperature after tool finishes cutting the workpiece, δ (s) is the air cutting time, T_0 is the room temperature and $a=0.3$ is cooling constant which is determined from Hosokawa *et al.* [25].

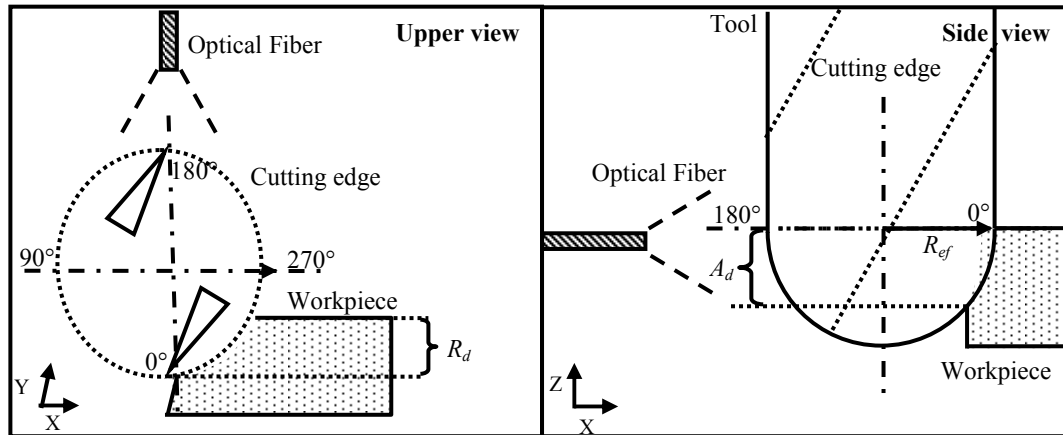


Figure 7 : Temperature Measurement Schematic

2.7 Characteristic Morphology of Metallic Powder

Table 1 shows characteristic morphology of metallic powder for laser sintered material.

Table 1: Characteristic morphology of metallic powder for laser sintered material

Materials	SCM	Ni	Cu
Powder Density (kg/m^3)	4690	4040	4690
Specific Heat (J/kgK)	450	490	380
Thermal Conductivity (W/mK)	0.13	0.17	0.17
Particle Diameter (μm)	30	30	30
Percent of Composition (%)	70	20	10

SCM : Carbon Molybdenum Steel

According to Yassin *et al.* [19], hardness and density of laser sintered material show increasing value when sintered with low energy density, $2.0 \text{ (J/mm}^2\text{)}$ to medium energy density, $9.0 \text{ (J/mm}^2\text{)}$. The values were increased from 211 ($\text{HV}_{0.3}$) to 275 ($\text{HV}_{0.3}$) for material hardness and $6950 \text{ (kgm}^{-3}\text{)}$ to $7680 \text{ (kgm}^{-3}\text{)}$ for material density. However, almost equal value of material hardness, 270 ($\text{HV}_{0.3}$) and density $7680 \text{ (kgm}^{-3}\text{)}$ obtained when the metallic powder was sintered with high-energy density, $20 \text{ (J/mm}^2\text{)}$. The laser sintered material properties were taken for the inner work material surface whereas metallic powder is fully melted due to heat and reheat processes which are 1.0 mm from the periphery surface [6].

2.8 Materials Properties and Cutting Conditions

Materials properties and cutting conditions are shown in Tables 2 and 3 [18, 19].

Table 2 : Materials Properties

Materials	WC (Tool)	LSMEp9	AISI 1055
Young Modulus, E (GPa)	650	124	250
Poisson Ratio, ϵ	0.25	0.3	0.3
Thermal Conductivity, k (W/mK)	15	10	53
Density, ρ (kg/m^3)	14900	7680	7850
Specific Heat, c (J/kgK)	334	450	486
Hardness Vickers, $\text{HV}_{0.3}$	1400	275	145

Table 3 : Cutting Conditions

Parameters	Values
Cutting tool Radius, R (mm)	0.3,0.5,1.0,3.0
Radial depth of cut, R_d (mm)	0.1-0.6
Revolution Speed (RPM)	4000-40000
Cutting speed, V_c (m/min)	75-754
Cutting feed, f (mm/tooth)	0.01

3.0 RESULTS AND DISCUSSION

3.1 Cutting Forces Analysis

Figure 8 shows cutting force profile obtained from the simulation result. A single peak value was taken as the analysis cutting force. Figure 9 shows the comparison of different shear friction models and different radial depths for AISI 1055 at 4000rpm.

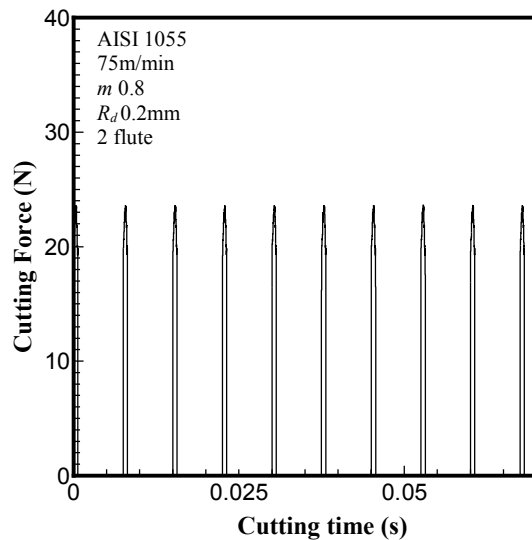


Figure 8: Cutting force profile

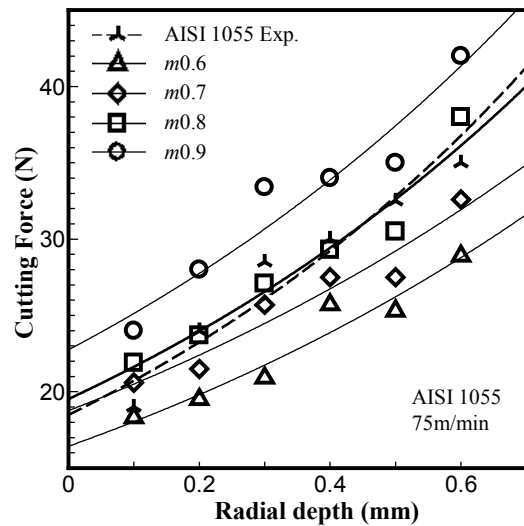


Figure 9 : Effect of frictions model and radial depth on cutting force

From Figure 9, shear friction factor, m and radial depth, R_d shows direct proportional effect on cutting force. This is due to increasing frictional stress on the rake face and chip removal rate (mm^3/s) during metal cutting. Shear friction factor 0.8 can be considered as the optimum shear friction model in estimating cutting force. This is due to lowest errors (5-15%) shown and according this shear friction model, high precision simulation results that related to cutting force such as cutting temperature could be obtained.

Figure 10 shows the cutting force comparison between simulation and experimental results for AISI 1055 and LSMEp9. The cutting processes were simulated by FEM with the same shear friction model of $m0.8$ and revolution speed 4000rpm for both materials. Cutting force of AISI 1055 is higher than LSMEp9 at the equal cutting rotational speed. This is because of LSMEp9 is easy to deform due to lower Young Modulus (124GPa) than AISI 1055 (250GPa).

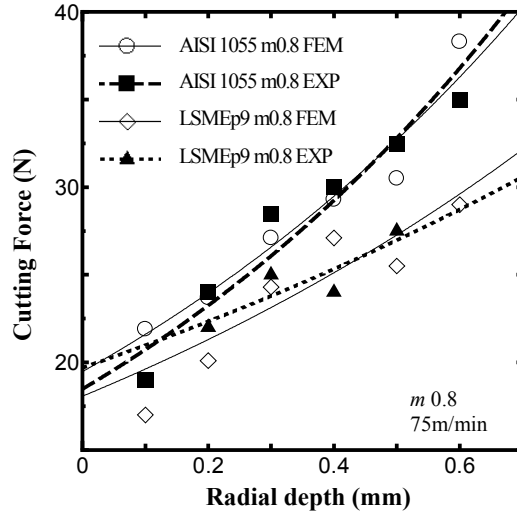


Figure 10 : Effect of Young modulus and radial depth on cutting force

3.2 Cutting Temperature Analysis

Figure 11 shows the temperature profile for machining LSMEp9 at 754m/min and 0.1mm radial depth at 0°. The single peak value was taken as analysis cutting temperature. After considering the cooling effect during ball end milling processes base on Equation 5, comparisons of estimated cutting temperature of AISI 1055 and LSMEp9 with experimental results are shown in Figure 12.

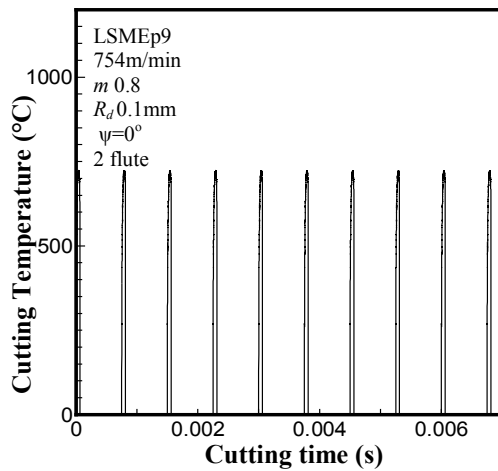


Figure 11: Cutting temperature profile

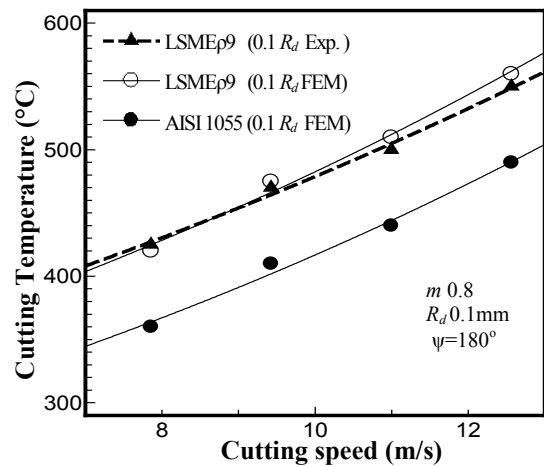


Figure 12 : Effect of cutting speed on cutting temperature

FEM simulation of LSMEp9 shows cutting edge temperature error below 5% as compared to the experimental results. From Figure 12, it is known that LSMEp9 shows higher temperature gradient than AISI 1055. This is due to the lower thermal conductivity of LSMEp9 (10 W/mK) than AISI 1055 (53 W/mK). Heat becomes more difficult to conduct away from heat source for material with low thermal conductivity.

This phenomenon can be explained in Figure 13 whereas steady state analyses for temperature distributions inside the workpiece when machining both materials at 754m/min was performed.

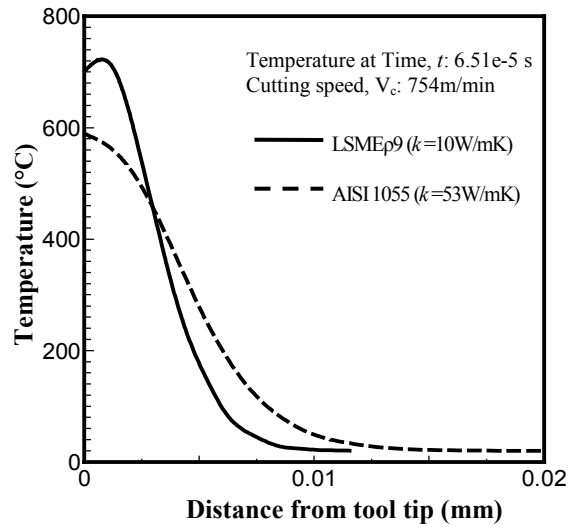


Figure 13 : Temperature distribution comparison for different thermal conductivity

Workpiece temperature near the tool tip for LSMEp9 is higher than AISI 1055. Nevertheless, cutting temperature decreases drastically for LSMEp9 workpiece along the cross sectional as compared to AISI 1055 workpiece. This is due to the quantity of heat travels inside LSMEp9 workpiece is lower than AISI 1055 in single unit time.

3.3 Different Tool Diameter Analysis

In this study, the effect of ball end mill diameter and cutting temperature, relationship of cutting speed and specific cutting force analysis were performed.

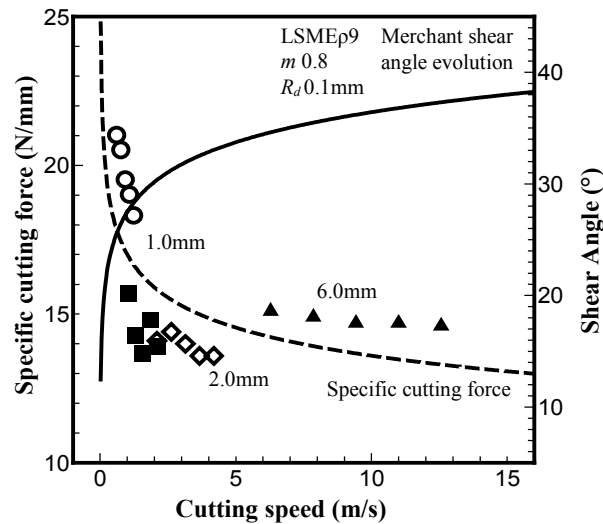


Figure 14 : Effect of cutting speed on specific cutting force and merchant shear angle evolution

Figure 14 shows the relationship between cutting force and Merchant shear angle evolution with increasing cutting speed during machining LSMEp9 for different cutting tool diameter. The Merchant shear angle evolution is obtained from Sutter *et al.* [26] is shown in Equation 6.

$$\theta_M = (0.5\pi - \zeta + \alpha)/2, \quad \zeta = 0.704V^{0.248} \quad (6)$$

From Figure 14, increasing cutting speed tend to decrease specific cutting force. Nevertheless, specific cutting force slightly decreases at highest cutting speed.

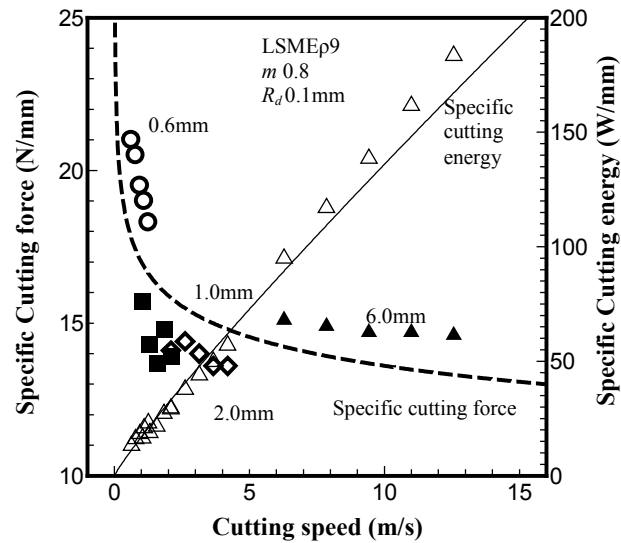


Figure 15: Effect of cutting speed on cutting force and cutting energy

This phenomenon in Figure 14 can be explained using Merchant shear angle evolution whereas shear angle drastically increase at lower cutting speed but slightly increase at higher cutting speed. It is well-known that shear angle have a direct effect on cutting force [27]. Figure 15 shows the relationship between cutting force and cutting energy with increasing cutting speed. It is known that increasing of cutting speed will increase cutting energy according to Equation 3. This analysis could explain the cutting force evolution and cutting energy at high cutting speed since it is impractically to obtain cutting forces during experiment due to measurement tool limitation [19].

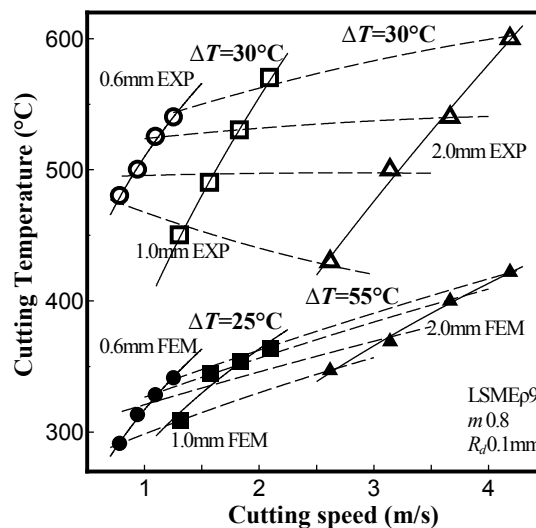


Figure 16: Comparison between estimated cutting temperatures with experiment

Figure 16 shows the comparison between estimated cutting tool temperatures with the experimental approach for machining LSMEp9 using less than 2mm ball end mill. The estimation cutting temperature had shown large errors as compared to experimental

approach. This is due to the estimated cutting temperatures were obtained under the ideal cutting process whereas other parameters such as tool wear are neglected.

According to Newby *et al.*, end milling operation that less than 1.6mm diameter are considered as micro end milling operation whereas the cutting tool suffer aggressive feed per tooth per radius compare to conventional milling operations [28]. This process could increase tool wear rate such as adhesive, chatter or flank wear for end mill less than 1.6mm and could be related to increasing cutting temperature during the experiment. Furthermore, LSMEp9 have high material hardness that could contribute tool wear rate and temperature increases.

Further investigation need to be performed in order to explain this phenomenon such as effect of tool wear on cutting temperature using finite element analysis.

4.0 CONCLUSION AND RECOMMENDATION

In this study, cutting force and cutting temperature were estimated using 2 dimensional orthogonal cutting with thermo-mechanical plane strain model. Shear friction factors range between 0.6-0.9 are used in the study and the results are compared with the experimental results in terms of maximum cutting force and cutting temperature.

From the study, 2D shear friction model, $m=0.8$ estimated cutting force with lowest errors (5-15%). The study shows that the cutting force increases with the increases in shear friction factor and radial depth of cut (R_d) due to increasing frictional stress and chip removal rate (mm^3/s). Cutting edge temperature increases with increasing cutting speed due to increasing cutting energy. Estimated cutting temperature for AISI 1055 and LSMEp9 shows below 5% errors when comparing with experimental results. AISI 1055 shows higher cutting force than laser-sintered materials, LSMEp9 due its higher Young modulus. However, LSMEp9 developed higher cutting edge temperature than AISI 1055 due to its lower thermal conductivity.

From the study, it is also observed that laser sintered material has low machinability as compared to mild steel, AISI 1055 due to its high cutting temperature and material hardness. Decreasing tool diameter will increase specific cutting force (N/mm) and decreasing specific cutting energy (W/mm) due to decreasing cutting speed. FEM simulation results show decreasing cutting temperature when cutting tool diameter decreases. When comparing cutting tool temperature for less than 2mm diameter ball end mill, the estimated cutting temperature shows large error as compared to experimental approach. This shown that the ball end milling process in the experimental approach was not an ideal cut whereas other parameters such as cutting tool life and tool wear must be investigate in the simulation in order to gain further knowledge in machining laser sintered materials LSMEp9 with high precision.

This paper emphasized the application of 2D orthogonal model in simulating high speed machining. For future investigation, 3D FEM simulation could be applied in obtaining more precise results and data.

NOMENCLATURES

A_d	Axial Depth of cut (mm)
a	Cooling ratio
b	Cutting width (mm)
δ	Cooling time (s)
F_v	Cutting force (N)
f	Feed rate (mm/tooth)
h	Heat transfer coefficient at tool-chip interface ($\text{kW}/\text{m}^2\text{K}$)
k	Normal stress (MPa)

m	Shear friction factor
Q_r	Heat Generation rate (W)
q	Heat Flux (W/m^2)
R	Tool radius (mm)
R_{ef}	Tool effective radius (mm)
R_d	Radial Depth of cut (mm)
r	Tool edge radius (mm)
T_ψ	Temperature at degree ($^{\circ}C$)
T_0	Temperature at 0 degree ($^{\circ}C$)
T_r	Room Temperature ($^{\circ}C$)
τ	Flow stress (MPa)
t	Cutting thickness (mm)
θ	Tool penetration angle ($^{\circ}$)
θ_M	Merchant Shear Angle ($^{\circ}$)
V	Cutting speed (m/s)
W_c	Machining work done (W)
ζ	Shear angle evolution factor

ACKNOWLEDGEMENT

Author would like to show greatest appreciation to Universiti Malaysia Pahang (UMP) and Kementerian Pengajian Tinggi (KPT) for funding the master study.

REFERENCES

1. Dewes R. C. and Aspinwall D. K., *A review of ultra high speed milling of hardened steels*. Journal of Materials Processing Technology, 1997. 69(1-3): p. 1-17.
2. King D. and Tansy T., *Rapid tooling: Selective laser sintering injection tooling*. Journal of Materials Processing Technology, 2003. 132(1-3): p. 42-48.
3. Ramada S. and Dickens P., *Rapid tooling analysis of Stereolithography injection mould tooling*. International Journal of Machine Tools and Manufacture, 2007. 47 (5): p. 740-747.
4. Kalpakjian S. and Schmidt S.R., *Manufacturing engineering and technology*. 4th ed., 2000. Prentice Hall International.
5. Guzzle B. U. and Lazuli I., *An enhanced force model for sculptured surface machining*. Machining Science and Technology, 2004. 8(3): p. 431-448.
6. Abe S., Higashi Y., Few I., Yoshida N., and Onokama T., *Milling-combined laser metal sintering system and production of injection molds with sophisticated function*. Proceeding of 11th International Conference on Precision Engineering, 2006. Tokyo, Japan.
7. Abe S., *Study on Development of Milling-Combined Laser Metal Sintering System and Production of Injection Molds*. Doctoral Thesis, Department of Mechanical System Engineering, Kanazawa University, Kanazawa, 2008. Ishikawa, Japan.
8. Armoring, E. J. A., Shi G., and Veers S., *Modeling the basic cutting action and machining performance of sintered metallic materials*. Machining Science and Technology, 2001. 5(3): p. 353-373.
9. Hamiuddin M. and Mustafa Q., *Machinability of phosphorous containing sintered steels*. Materials Chemistry and Physics, 2001. 67(1-3): p. 78-84.

10. Filice L., Micari F., Rizzuti S., Umbrello D., *Dependence Of Machining Simulation effectiveness On Material And Friction Modelling*. Machining Science and Technology, 2008. 12(3): p. 370-389.
11. Ozel T., *The Influence of Friction Models On Finite Element Simulations of Machining*, Int. Journal of Tools and Manufacturing, 2006. 46: p. 518-530.
12. Usui E. and Shirakashi T., *Mechanics of Machining from Descriptive to Predictive Theory*. The Art of Cutting Metals- 75 Years Later- ASME PED, 1982. 7: p. 13-55.
13. Strenkowski J. S., and Carroll J. T., *A Finite Element Model of Orthogonal Metal Cutting*. Trans. ASME Journal of Engineering for Industry, 1985. 107: p. 346-354.
14. Davim J. P., and Maranhao C., *A Study of Plastic Strain and Plastic Strain Rate in Machining of Steel AISI 1045 Using FEM Analysis*. Materials and Design, 2009. 30: p. 160-165.
15. Davim J. P., Maranhao C., Jackson M. J., Cabral G., Gracio J., *FEM analysis in high speed machining of aluminium alloy (Al7075-0) using polycrystalline diamond (PCD) and cemented carbide (K10) cutting tools*. International Journal of Advanced Manufacturing Technology, 2008. 39: p. 1093-1100
16. Umbrello D., *Finite element simulations of conventional and high speed machining of Ti6Al4V alloy*. Journal of Materials Processing Technology, 2008. 196(1-3): p. 79-87.
17. Ozel T., Altan T., *Process simulation using finite element method - prediction of cutting forces, tool stresses and temperature in high speed flat end milling*. International Journal of Machine Tools & Manufacturing, 2000. 40: p. 713-718.
18. Furumoto T., Ueda T., Abdul Aziz M. S., Hosokawa A., Tanaka R., *Study on reduction of residual stress induced during rapid tooling process – influence of heating conditions on residual stress*. Key Engineering Materials, 2010. 447-448: p. 785-789.
19. Yassin A., Ueda T., Furumoto T., Hosokawa A., Tanaka R., Abe S., *Experimental investigation on cutting mechanism of laser sintered material using small ball end mill*. Journal of Materials Processing Technology, 2009. 209: p. 5680-5689.
20. Ergatoudis I., Irons B. M. and Zienkiewics O. C., *Curved, isoparametric 'Quadrilateral' element for finite element analysis*. International Journal of Solids Structures, 1968. 4, p. 31-42.
21. Kato S., Yamaguchi K., Yamada M., *Stress distribution at the interface between tool and chip in machining*. Trans. ASME Journals of Engineering for Industry, 1972. 94: p. 683-689.
22. Abukhshim N. A., Mativenga P. T., Sheikh M.A., *Heat generation and temperature prediction in metal cutting: review and implications for high speed machining*. International Journal of Machine Tools & Manufacture, 2006. 46: p. 782-800.
23. Coelho R. T., Ng E. G. , Elbestawi M. A., *Tool wear when turning hardened AISI 4340 with coated PCBN tools using finishing cutting conditions*. International Journal of Machine Tools and Manufacture, 2007. 47(2): p. 263-272.
24. Abukhshim N. A., Mativenga P. T., Sheikh M. A., *Investigation of heat partition in high speed turning of high strength alloy steel*. International Journal of Machine Tools & Manufacture, 2005. 45: p. 1687-1695.
25. Hosokawa A., Zhou Z. P., Yamada K. and Ueda T., *Studies on High-speed Milling with Small Ball End Mill: Temperature Distribution on Flank Face of Cutting Tool*. Journal of Japanese Society Precision Engineering, 2010. 70(12): p. 1527-1532.
26. Sutter G., *Chip geometries during high-speed machining for orthogonal cutting conditions*. International Journal of Machine Tools & Manufacture, 2005. 45: p. 719-726.

27. Trent E., Wright P., *Metal Cutting*, 4th ed., 2000. Butterworth Heinemann, US.
28. Newby G., Venkatachalan S., Liang S. Y., *Empirical analysis of cutting force constants in micro-end-milling operations*. *Journal of Materials Processing Technology*, 2007. 192-193: p. 41-47.